Supporting Information

Krick et al. 10.1073/pnas.1205128109

SI Materials and Methods

Purification and Crystallization of KlHsv2. The DNA encoding *Kluyveromyces lactis* KlHsv2 (UniProt entry Q6CN23) was codon-optimized for *Escherichia coli* expression, chemically synthesized (Mr. Gene), and cloned into the pET-28a vector (Novagen). The protein was expressed with an N-terminal 6 × His-tag in *E. coli* BL21(DE3) in ZYM-5052 autoinducing medium (1) for 3 h at 37 °C and then overnight at 25 °C. After harvesting, the cells were resuspended in 30 mM imidazole, 0.4 M NaCl, and 50 mM NaH_2PO_4 (pH 7.5) (buffer A). After lysis through sonication, the supernatant was applied onto a 1-mLHisTrap column (GE Healthcare) and eluted with a gradient from 0 to 100% B [0.4 M imidazole, 0.4 M NaCl, 50 mM NaH_2PO_4 (pH 7.5)]. KlHsv2 was then dialyzed against gel filtration buffer [0.2 M NaCl, 30 mM sodium citrate (pH 5.5)], concentrated, and loaded onto a Superdex 200 16/60 column (GE Healthcare). Selenomethionine-substituted KlHsv2 was expressed in minimal medium supplemented with selenomethionine in *E. coli* as described (2) and purified as the native protein. Purified proteins were concentrated, flash-frozen in liquid nitrogen, and stored at −80 °C.

For crystallization, 200 nL of 36 mg/mL KlHsv2 was mixed with 200 nL of the precipitant, 1.6 M $MgSO_4$, 0.1 M Mes (pH 6.5), and 40 nL of 0.15 mM CYMAL-7 from the Additive Screen (Hampton Research) in a sitting drop MRC crystallization plate (Molecular Dimensions) using a Cartesian pipetting robot (Zinsser Analytic). Crystals were grown at 20 °C and then transferred into a cryoprotectant consisting of 20% ethylene glycol, 1.6 M $MgSO_4$, and 0.1 M Mes (pH 6.5), and flash-cooled in liquid nitrogen. For soaking experiments, crystals were gradually transferred into a solution consisting of 1.6 M sodium malonate and 0.1 M Mes (pH 6.5) to remove the sulfate ions from the crystallization buffer. The crystals were then soaked in a cryoprotectant consisting of 15% ethylene glycol, 1.6 M sodium malonate, 0.1 M Mes (pH 6.5), and 2.2 mM inositol-1,3,5-triphosphate (Avanti Polar Lipids). Crystals were soaked for 1.5 min at 20 °C and then flash-cooled in liquid nitrogen. However, no ligand bound (Table 1). Selenomethionine crystals were grown with the hanging drop method using 24-well Linbro plates. A total of 1.5 μL of 20 mg/mL selenomethionine-labeled KlHsv2 was mixed with 1 μL of 1.6 M $MgSO_4$ and 0.1 M Mes (pH 6.7) and kept at 20 °C. After transfer of the crystals into the cryoprotectant [20% glycerol, 1.6 M $MgSO_4$, 0.1 M Mes (pH 6.7)], they were flash-cooled in liquid nitrogen.

Data Collection and Structure Determination. Diffraction data of cryocooled crystals were collected at 100 K at beamline X10SA (Swiss Light Source, Paul Scherrer Institute, Villigen, Switzerland). Data were processed and scaled with the XDS software package (3). The structure was determined by single-wavelength anomalous diffraction phasing using the data collected from a selenomethionine-substituted KlHsv2 crystal. Six of seven Se sites were found with SHELXD/HKL2MAP (4, 5) and yielded a solution with an overall correlation coefficient of 51.1%. An interpretable electron density map was obtained after density modification with SHELXE/HKL2MAP. Automated model building was done with ArpWarp (6). The graphics program Coot (7) was used for manual model building, and refinement was carried out with Refmac5 (8) and Phenix (9). The final model was refined to a R_{work}/R_{free} of 19.7%/24.3% at a resolution of 3.0 Å and comprises residues 14–269 and 275–338. Figures were prepared with PyMOL (10).

Liposome Flotation Assays. ScHsv2 alanine mutants were prepared with the QuikChange II Site-Directed Mutagenesis Kit (Stratagene). ScHsv2 mutants were expressed as GST fusion proteins from the pGEX-4T-3 vector in *E. coli* BL21(DE3). Proteins were purified with a 5-mL GSTrap FF column (GE Healthcare) using standard buffer [300 mM NaCl, 30 mM Hepes (pH 7.0)]. GST-fusion proteins were eluted with 20 mM glutathione in standard buffer. The GST tag was cleaved off with thrombin, and after dialysis against standard buffer, free GST was removed through a second GSTrap FF column run. The ScHsv2 mutants were then concentrated and applied onto a Superdex 75 column 16/60 (GE Healthcare). Purified proteins were concentrated and flash-frozen in liquid nitrogen.

Protein binding to liposomes was investigated with flotation assays as described previously (11, 12). For preparation of liposomes, a 1-mg containing lipid mix composed of 73% (wt/wt) L-phosphatidylcholine isolated from chicken egg (840051C; Avanti Polar Lipids); 2% Texas Red–1,2-dihexadecanoyl-*sn*-glycero-3-phosphoethanolamine (DHPE), triethylammonium salt (T1395MP; Invitrogen); 23% L-phosphatidylethanolamine (brain, porcine; 840022P; Avanti Polar Lipids); and 2% phosphatidylinositol-3-phosphate (1,2-dioleoyl-*sn*-glycero-3-phospho-[1′-myo-inositol-3′-phosphate]), ammonium salt (850150P; Avanti Polar Lipids) was pipetted together and dried. Dried lipids were resuspended in with 50 μL of HP150 buffer containing 5% cholate and then 100 μL of HP150 with 1.5% cholate. HP150 buffer consists of 150 mM KCl and 20 mM Hepes (pH 7.4). Cholate was removed by size exclusion chromatography using a self-packed column filled with 0.5 g of Sephadex G50 (Sigma) resuspended in HP150 buffer. Liposome-containing fractions were pooled and stored at 4 °C.

Five microliters of 1.5 μM protein was incubated with 45 μL of liposomes at room temperature for 10 min. The protein-liposome mixture was then mixed with 50 μL of 80% Nycodenz (wt/vol in HP150 buffer) and overlaid with 50 μL of 30% Nycodenz (Progen) in 7-mm × 20-mm PC tubes (Beckman). The gradient was covered with 30 μL of HP150 buffer. The samples were centrifuged at 55,000 rpm for 1.5 h at 4 °C in a Sorvall S55S-1190 rotor (Thermo Scientific) with a Sorvall Discovery M150SE analytical ultracentrifuge (Thermo Scientific). Thirty-microliter samples were taken starting from top of the gradient and analyzed by Western blotting using a polyclonal rabbit antibody raised against a ScHsv2 C-terminal peptide (CGEPTRWELVRESWREL).

Isolation of GST-ScHsv2. Plasmids were transformed into *Escherichia coli* BL21 containing the lysozyme-expressing plasmid pLysS (M. Rose, Molecular Genetics and Cellular Microbiology, University of Frankfurt, Frankfurt, Germany). Cells containing both plasmids were grown in LB with ampicillin (75 μg/mL) and chloramphenicol (25 μg/mL) to an OD_{600} of 0.5–0.8, induced with isopropyl-β-D-thiogalactopyranoside (0.1 mM, 2–4 h at 30 °C), harvested, snap-frozen, and stored at −80 °C. Cells were resuspended in ice-cold PBS containing protease inhibitor mixture (Sigma), 10 mM $MgCl_2$, DNase I (Invitrogen), and 1% Triton X-100. Supernatants from lysed cells (15 min, 8000 × g at 4 °C) were applied to glutathione–Sepharose 4B beads (30–50 min at 4 °C). Elution followed the manufacturer's recommendations. Protein concentration was determined using the Bradford method, and quality of the protein preparation was verified by gel analysis using Coomassie staining.

Lipid Blots. PIP-Strips (Echelon Biosciences) were processed as described by Krick et al. (13), except that 3% BSA was used for blocking. Blocking was done for 30 min [3% BSA, 50 mM Tris·HCl (pH 7.5), 0.5 mM $MgCl_2$], and it was then incubated with 100 ng/mL GST-fusion protein [50 mM Tris·HCl (pH 7.5), 0.5 mM $MgCl_2$] for 1 h, followed by an antibody against GST [1:5,000 in 3% BSA, 50 mM Tris·HCl (pH 7.5), 0.5 mM $MgCl_2$] and an antibody conjugated to HRP (1 h).

Reflectometric Interference Spectroscopy Experiments. Reflectometry was used to determine the binding affinity of GST-ScHsv2 WT and five mutants to PtdIns3P in a lipid membrane. For this purpose, silicon wafers with an oxide layer with a thickness of 5 μm were used, which supply a sufficiently thick film for interference fringes. Before the measurement, the wafers were cleaned in an aqueous solution of ammonia and hydrogen peroxide (5:1:1, 15 min at 70 °C) and treated with oxygen plasma for 1 min. Small unilamellar vesicles (SUVs) were prepared from 1,2-dioleoyl-*sn*-glycero-3-phosphatidylcholine and 1,2-dioleoyl-*sn*-glycero-3-phospho-[1′-myo-inositol-3′-phosphate], ammonium salt (PtdIns3P; 850150P) in a molar ratio of 97:3 [10 mM Hepes, 150 mM NaCl (pH 6.5), c = 1 mg/mL] via sonication. Lipids were purchased from Avanti Polar Lipids.

Spectra were recorded every 2 s with a NanoCalc-2000-Vis/NIR spectrometer (Ocean Optics). The data were evaluated online with a self-written MATLAB tool. A baseline was recorded by placing a wafer in a flow cell and rinsing the system with the buffer mentioned above for 5 min. Lipid membranes were spread on the wafer by rinsing the SUV solution through the cell. Excess of vesicles was removed by extensive rinsing with 10 mM Hepes and 150 mM NaCl buffer at pH 7.5. After the measurement signal stabilized, the protein in question was added to the flow-through system. The concentration was increased stepwise either after equilibrium was reached for each addition of protein or after at least 5 min passed without significant change of the measurement signal. At the end of each measurement, the system was excessively rinsed with the buffer mentioned above. The binding affinity was determined by plotting the rise in optical thickness against the concentration and applying a Langmuir-fit to the curve.

Isothermal Titration Caliometry Measurements. Liposomes were prepared in the same manner as for the liposome flotation assays and were composed of 2% PtdIns3P, 73% phosphatidylcholine, 23% phosphatidylethanolamine, and 2% Texas Red phophatidylethanolamine. We determined the phosphate content of the prepared liposomes using the phosphomolybdate method (14) to calculate the PtdIns3P concentration. For our calculations, we assumed that all phospholipids were equally well incorporated into the liposomes and took into account that PtdIns3P contains two phosphate groups and the other phospholipids contain a single phosphate group per molecule. Based on an average radius of 18 nm for liposomes prepared with this protocol (15) and a thickness of 6 nm for the lipid bilayer, we calculated that 60% of the total PtdIns3P is accessible on the surface of the liposomes.

For isothermal titration calorimetry (ITC) measurements, ScHsv2 was dialyzed into HP150 buffer. ITC measurements were done with a VP ITC MicroCalorimeter (MicroCal) at 25 °C. Protein was titrated into liposomes. Titrations were carried out with 20-fold 15-μL injections, and the first injection was 3 μL. Protein concentrations used for measurements were in the range of 50–90 μM, and calculated accessible PtdIns3P concentrations were in the range of 5–10 μM. Data were fitted with a single-site binding model using the MicroCal Origin 7.0 software.

Cloning and Mutagenesis. Mutagenesis of pRS313-Atg18-HA was carried out by overlapping extension PCR using mutagenesis primers and I and *EcoR*I as cloning sites into pRS313 [OEP-Atg18 SalI forward (for), OEP-Atg18 EcoRI reverse (rev)]. Double-mutant Atg18 S264A H315A was created by two successive rounds of PCR, and Atg18 Penta (S264A, R285A, and H244A out of binding site 1 and R286A and H315A out of binding site 2) was created with multiple rounds of mutagenesis. GST-Hsv2 was cloned by PCR using the primers GFP-Ygr223c f and GFP-Ygr223c r and ligation into pUG36 by the *BamH*I and XhoI sites. Point mutations were introduced using the QuikChange II-Site-Directed Mutagenesis Kit (Stratagene). GFP-Hsv2 and the corresponding mutants were constructed by cleaving the GST fusions with *BamH*I and XhoI, followed by ligation into pGEX4-T3 (Amersham). GFP-Atg18 and the corresponding mutants were constructed by isolating the insert with PCR using the primers GFP-Atg18 Eco for and GFP-Atg18 Xho rev and cleavage by *EcoRI* and *XhoI*, followed by ligation into the corresponding cleavage sites of pUG36.

Monitoring of the Autophagic Rate. An *atg18*Δ strain (16) in the WCG4α background (Matα *ura3 his3-11,15 leu2-3,112*) (17) was transformed with pRS313-Atg18-HA or the corresponding mutants and pRS316-PGK1-GFP (18). The plasmid pRS313-Atg18-HA was constructed by isolation of the endogenous promotor region of Atg18 and the HA-tagged Atg18 ORF from cen-ATG18-HA (19) using *Xba*1 and *Sal*1 in ligation into pRS313. *ATG18* cloned from our laboratory background differs from the database sequence in one nucleotide leading to substitution of threonine 7 to an isoleucine, without affecting functionality. The autophagic rate was determined using PGK1-GFP as marker protein as described (18). The autophagic rate of the WT Atg18-HA after 6 h of starvation was set to 100%. The SEM was calculated from five independent experiments. The percentage of mApe1 was determined from the total amount of pApe1 and mApe1 at time point zero. SEM was calculated. Quantification was done using AIDA software (Raytest). Samples were immunoblotted using a GFP antibody (Roche), anti-proaminopeptidase I Ape1 antibody (20), and an HA antibody (Santa Cruz Biotechnology) to control protein stability. Second antibodies were HRP-conjugated goat anti-rabbit (Medac) and HRP-conjugated goat anti-mouse (Dianova).

Fluorescence Microscopy. *S. cerevisiae atg18Δ::KanMX6* cells (16) were transformed with *MET25*::GFP-ScAtg18 or the corresponding mutants and pRS425-RFP-ScAtg8. A S288C strain expressing chromosomally tagged Snf7-RFP (21) was transformed with either *MET25*::GFP-ScAtg18 variants or *MET25*::GFP-Hsv2 variants. Cells were grown to stationary phase in medium containing 0.3 mM methionine to induce endogenous proteins levels. A DeltaVision Spectris (Applied Precision) fluorescence microscope equipped with a 100× objective and FITC and TRITC filter set (excitation wavelengths of 340–380 and 465–495 and emission wavelengths of 435–485 and 515–555, respectively) was used. Pictures were taken and deconvoluted using WoRx (Applied Precision) software and processed using Adobe Systems Photoshop.

For the analysis of vacuolar fragmentation, *S. cerevisiae atg18Δ:: KanMX6* cells of the BY4741 background (Euroscarf) were transformed with the indicated pRS313-ScAtg18-HA constructs. Vacuolar membrane staining was done using 32 μM *N*-(3-triethylammoniumpropyl)-4-(*p*-diethylaminophenylhexatrienyl) pyridinium dibromide (FM4-64; Invitrogen) for 30 min. Pictures were taken using a Zeiss Axioskope 2 with the FITC filter set. Digital images were taken using an AxioCam MRm camera and AxioVision software (version 4.5; Zeiss). Images were processed with Photoshop.

Simulation and Docking Studies. ***Simulation studies.*** The GROMACS 4.5.4 simulation package (22, 23) was used for the molecular dynamics (MD) simulation, with the GROMOS96 43a2 (24) force field and the simple point charge (SPC) (25) water model.

Periodic boundary conditions were applied to the system. Long-range electrostatics were calculated using the particle mesh Ewald (PME) method (26, 27) with a real-space cutoff of 10 Å. For the van der Waals interactions, a cutoff of 10 Å was used. The simulation was performed at 300 K using the V-rescale modified Berendsen thermostat (28) with a coupling constant τ_T of 0.1 ps. A constant pressure of 1 bar was maintained using a Parrinello–Rahman bariostat (29) in an isotropic coupling type with a coupling constant τ_p of 2 ps and a compressibility of 4.5×10^{-5} bar^{-1}. The integrator for the simulation was leap-frog integrator with a step of 2 fs. The LINCS method (30) was used to constrain bond lengths. Coordinates were saved every 2 ps for analysis.

For MD, the 3.35-Å resolution KlHsv2 crystal structure was used. This structure contains residues 270–274, part of the loop connecting strands C and D of blade 5, which are missing in the 3.0-Å crystal structure. Side chains, which are disordered in the crystal structure, were added to the model with conformations that do not cause steric clashes with Coot. H178 and H249 of KlHsv2 were protonated for the MD simulation using GROMACS tools. Next, energy minimization was done in vacuo, first using steepest descent followed by a conjugate gradient energy minimization. The protein was solvated and charge-neutralized. The system was then energy-minimized, and two position-restrained simulations of 100 ps each were performed for temperature (canonical ensemble) and pressure (isothermic-isobaric ensemble) equilibration. A production run was done for 30 ns. PyMOL (10) was used for visualization.

Docking studies. Autodock 4.2 (31) was used for the docking studies. The topology of PtdIns3P and PtdIns(3,5)P_2 was obtained using the PRODRG server (32), yielding total charges of −3 and −5, respectively. The ligands were allowed torsional flexibility, whereas the macromolecule was kept rigid. H178 and H249 were protonated for all docking studies. To sample the flexibility of the macromolecule, the ligands were docked in seven snapshots taken each 5 ns from a 30-ns MD simulation of KlHsv2. Grid boxes were centered in the two binding sites. The default grid spacing of 0.375 Å was used. The Lamarckian genetic algorithm (31, 33) with 2,500,000 evaluations and 100 runs was used for docking. The schematic diagrams of protein-ligand interactions were visualized with LIGPLOT v.4.5.3 (34).

1. Studier FW (2005) Protein production by auto-induction in high density shaking cultures. *Protein Expr Purif* 41:207–234.
2. Van Duyne GD, Standaert RF, Karplus PA, Schreiber SL, Clardy J (1993) Atomic structures of the human immunophilin FKBP-12 complexes with FK506 and rapamycin. *J Mol Biol* 229:105–124.
3. Kabsch W (1993) Automatic processing of rotation diffraction data from crystals of initially unknown symmetry and cell constants. *J Appl Cryst* 26:795–800.
4. Pape T, Schneider TR (2004) HKL2MAP: A graphical user interface for macromolecular phasing with SHELX programs. *J Appl Cryst* 37:843–844.
5. Sheldrick GM (2008) A short history of SHELX. *Acta Crystallogr A* 64:112–122.
6. Perrakis A, Morris R, Lamzin VS (1999) Automated protein model building combined with iterative structure refinement. *Nat Struct Biol* 6:458–463.
7. Emsley P, Cowtan K (2004) Coot: Model-building tools for molecular graphics. *Acta Crystallogr D Biol Crystallogr* 60:2126–2132.
8. Murshudov GN, Vagin AA, Dodson EJ (1997) Refinement of macromolecular structures by the maximum-likelihood method. *Acta Crystallogr D Biol Crystallogr* 53: 240–255.
9. Adams PD, et al. (2010) PHENIX: A comprehensive Python-based system for macromolecular structure solution. *Acta Crystallogr D Biol Crystallogr* 66:213–221.
10. Schrodinger, LLC (2010) The PyMOL Molecular Graphics System (Schrodinger, Portland, OR), Version 1.3r1.
11. Matsuoka K, et al. (1998) COPII-coated vesicle formation reconstituted with purified coat proteins and chemically defined liposomes. *Cell* 93:263–275.
12. Weber T, et al. (1998) SNAREpins: Minimal machinery for membrane fusion. *Cell* 92: 759–772.
13. Krick R, Tolstrup J, Appelles A, Henke S, Thumm M (2006) The relevance of the phosphatidylinositolphosphat-binding motif FRRGT of Atg18 and Atg21 for the Cvt pathway and autophagy. *FEBS Lett* 580:4632–4638.
14. Eibl H, Lands WE (1969) A new, sensitive determination of phosphate. *Anal Biochem* 30:51–57.
15. van den Bogaart G, et al. (2010) One SNARE complex is sufficient for membrane fusion. *Nat Struct Mol Biol* 17:358–364.
16. Barth H, Meiling-Wesse K, Epple UD, Thumm M (2001) Autophagy and the cytoplasm to vacuole targeting pathway both require Aut10p. *FEBS Lett* 508: 23–28.
17. Thumm M, et al. (1994) Isolation of autophagocytosis mutants of Saccharomyces cerevisiae. *FEBS Lett* 349:275–280.
18. Welter E, Thumm M, Krick R (2010) Quantification of nonselective bulk autophagy in S. cerevisiae using Pgk1-GFP. *Autophagy* 6:794–797.
19. Meiling-Wesse K, et al. (2004) Atg21 is required for effective recruitment of Atg8 to the preautophagosomal structure during the Cvt pathway. *J Biol Chem* 279:37741–37750.
20. Barth H, Meiling-Wesse K, Epple UD, Thumm M (2002) Mai1p is essential for maturation of proaminopeptidase I but not for autophagy. *FEBS Lett* 512:173–179.
21. Huh WK, et al. (2003) Global analysis of protein localization in budding yeast. *Nature* 425:686–691.
22. Hess B, Kutzner C, van der Spoel D, Lindahl E (2008) GROMACS 4: Algorithms for highly efficient, load-balanced, and scalable molecular simulation. *J Chem Theory Comput* 4:435–447.
23. Van Der Spoel D, et al. (2005) GROMACS: Fast, flexible, and free. *J Comput Chem* 26: 1701–1718.
24. van Gunsteren WF, et al. (1996) *Biomolecular Simulation: The GROMOS96 Manual and User Guide* (Vdf Hochschulverlag AG an der ETH, Zurich), p 1042.
25. Hermans J, Berendsen HJC, Vangunsteren WF, Postma JPM (1984) A consistent empirical potential for water-protein interactions. *Biopolymers* 23:1513–1518.
26. Darden T, York D, Pedersen L (1993) Particle mesh Ewald—An N.Log(N) method for Ewald sums in large systems. *J Chem Phys* 98:10089–10092.
27. Essmann U, et al. (1995) A smooth particle mesh Ewald method. *J Chem Phys* 103: 8577–8593.
28. Bussi G, Donadio D, Parrinello M (2007) Canonical sampling through velocity rescaling. *J Chem Phys* 126:014101.
29. Nose S, Klein ML (1983) Constant pressure molecular-dynamics for molecular-systems. *Mol Phys* 50:1055–1076.
30. Hess B, Bekker H, Berendsen HJC, Fraaije JGEM (1997) LINCS: A linear constraint solver for molecular simulations. *J Comput Chem* 18:1463–1472.
31. Morris GM, et al. (2009) AutoDock4 and AutoDockTools4: Automated docking with selective receptor flexibility. *J Comput Chem* 30:2785–2791.
32. van Aalten DMF, et al. (1996) PRODRG, a program for generating molecular topologies and unique molecular descriptors from coordinates of small molecules. *J Comput Aided Mol Des* 10:255–262.
33. Goodsell DS, Morris GM, Olson AJ (1996) Automated docking of flexible ligands: Applications of AutoDock. *J Mol Recognit* 9:1–5.
34. Wallace AC, Laskowski RA, Thornton JM (1995) LIGPLOT: A program to generate schematic diagrams of protein-ligand interactions. *Protein Eng* 8:127–134.

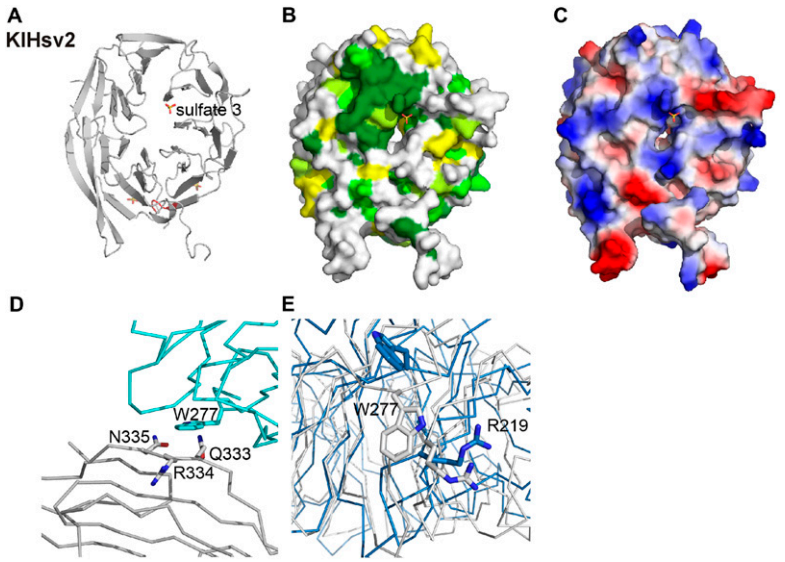

Fig. S1. Structure of KlHsv2. (*A*) Cartoon representation of the bottom view of KlHsv2. Sulfate 3 is labeled. The conserved FRRG motif is colored red in the cartoon representation. (*B*) Surface conservation of KlHsv2. The molecule is shown in the same orientation as in *A*. (*C*) Electrostatic surface potential of the same orientation. (*D*) In the crystal lattice, the aromatic side chain of W277 stacks against the C-terminal end of a symmetry-related molecule (gray). (*E*) MD simulation studies show that W277 swings away from binding site 2, whereas R219 remains orientated toward sulfate binding site 2. The KlHsv2 structure was solvated and simulated for 30 ns. The final structure (blue) is overlaid with the initial crystal structure (gray). The initial positions of W277 and R219 are shown in gray, and their final conformations after MD simulation are shown in blue.

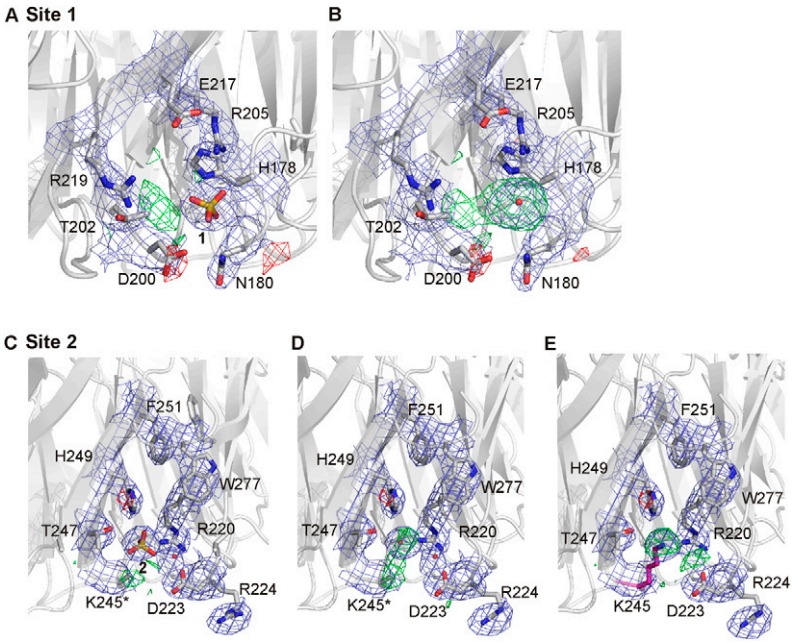

Fig. S2. Electron density maps of sulfate binding sites 1 and 2. (*A*) Close-up view of sulfate site 1. The final 3.0-Å resolution 2mFo-DFc electron density map is contoured at 1.0 σ (blue), and the final mFo-DFc difference map is contoured at both +3.0 σ (green) and −3.0 σ (red). The positive density left of the sulfate was modeled as water; however, after refinement, no density in the 2mFo-DFc map was observed for this water, and it was therefore deleted. (*B*) When a water molecule is included instead of a sulfate ion at site 1, positive density remains in the difference (mFo-DFc) map, which is contoured at +3.0 σ (green) and −3.0 σ (red). (*C*) Close-up view of sulfate site 2. The final 3.0-Å resolution 2mFo-DFc electron density map contoured at 1.0 σ (blue) and the final mFo-DFc map contoured at +3.0 σ (green) and −3.0 σ (red) are overlaid with the structure. (*D*) When a water molecule is included instead of a sulfate ion at site 2, positive density remains in the mFo-DFc map, which is contoured at +3.0 σ (green) and −3.0 σ (red). (*E*) Disordered side chain of K245 was included (magenta); however, positive density was observed in the difference map [contoured at +3.0 σ (green) and −3.0 σ (red)] after refinement. Therefore, K245 does not account for this density, and it is indeed a sulfate ion, which is bound at this site.

Fig. S3. Sequence alignment of Atg18 family members. PROPPINS from *S. cerevisiae*, *K. lactis,* human, and *Dictyostelium discoideum* were aligned with JalView and MAFFT (1). The Clustal color scheme is used.

1. Waterhouse AM, Procter JB, Martin DMA, Clamp M, Barton GJ (2009) Jalview Version 2—A multiple sequence alignment editor and analysis workbench. *Bioinformatics* 25:1189–1191.

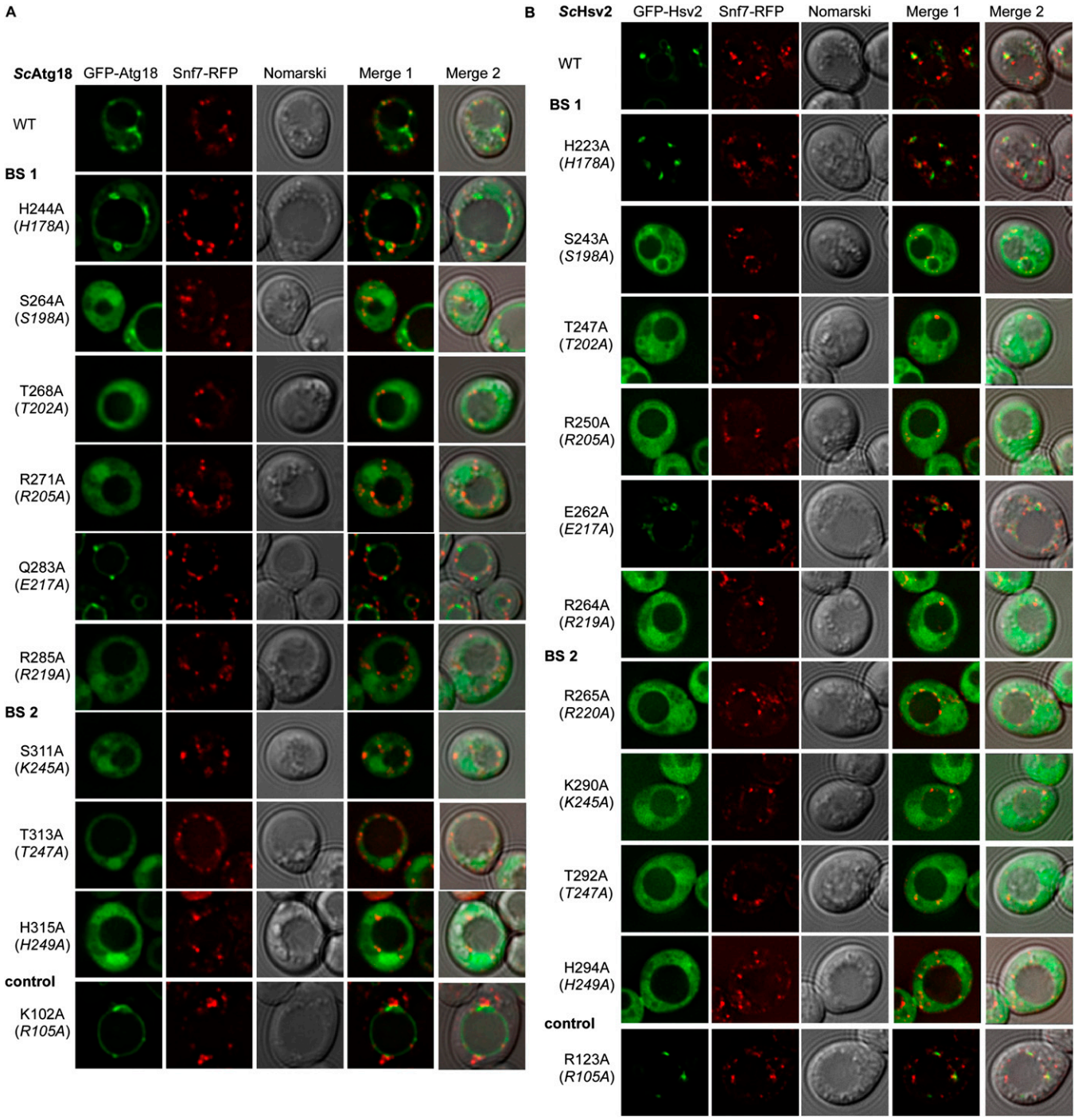

Fig. S4. Fluorescence microscopy analysis of membrane association of ScAtg18 and ScHsv2 mutants. Analysis of binding of GFP-ScAtg18 mutants (*A*) and GFP-ScHsv2 mutants (*B*) with endosomal structures. For each mutant, we included the corresponding KlHsv2 mutant in parentheses below. Cells chromosomally expressing Snf7-RFP are transformed with the indicated GFP-ScAtg18 (*A*) or GFP-ScHsv2 (*B*) plasmids and grown to stationary phase in selection medium containing 0.3 mM methionine to induce endogenous protein levels of GFP-fusion proteins. The GFP-Atg18 and GFP-Hsv2 WT proteins are recruited to PtdIns3P-positive endosomal structures labeled by the endosomal marker Snf7-RFP. The mutant proteins GFP-Atg18^{K102A} and GFP-Hsv2^{R123A}, which bear a mutation in a conserved patch opposite to the phosphoinositide binding motifs, were used as controls. Four mutations affecting the putative binding site 1 result in the release of the proteins to the cytosol for both ScAtg18 and ScHsv2 (ScAtg18: S264A, T268A, R271A, and R285A and ScHsv2: S243A, T247A, R250A, and R264A). Two mutants of site 1 (ScAtg18: H244A and Q283A and ScHsv2: H223A, and E262A) localize to WT-like green punctate structures. Four amino acids of sulfate binding site 2 are essential for membrane association in both proteins (ScAtg18: R286A, S311A, T313A, and H315A and ScHsv2: R265A, K290A, T292A, and H294A).

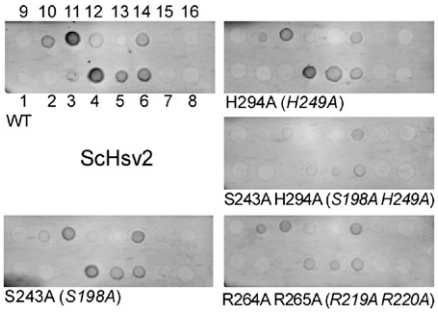

Fig. S5. Protein lipid overlay assays with GST-ScHsv2. Equal amounts of purified GST-ScHsv2 fusion protein, GST-ScHsv2^{S243A}, GST-ScHsv2^{H294A}, GST-ScHsv2$^{S243A\ H315A}$, and GST-ScHsv2$^{R264A\ R265A}$ were incubated with PIP-Strips. Bound GST fusion proteins were detected with a GST antibody: Lipids spotted on the membrane: 1, lysophosphatidic acid; 2, lysophosphocholine; 3, PtdIns; 4, PtdIns3P; 5, PtdIns4P; 6, PtdIns5P; 7, phosphatidylethanolamine; 8, phosphatidylcholine; 9, sphingosine-1-phosphate; 10, PtdIns(3,4)P_2; 11, PtdIns(3,5)P_2; 12, PtdIns(4,5)P_2; 13, PtdIns(3,4,5)P_3; 14, phosphatidic acid; 15, phosphatidylserine; 16, blank. One of three experiments is shown. The corresponding KlHsv2 residues are shown in parentheses.

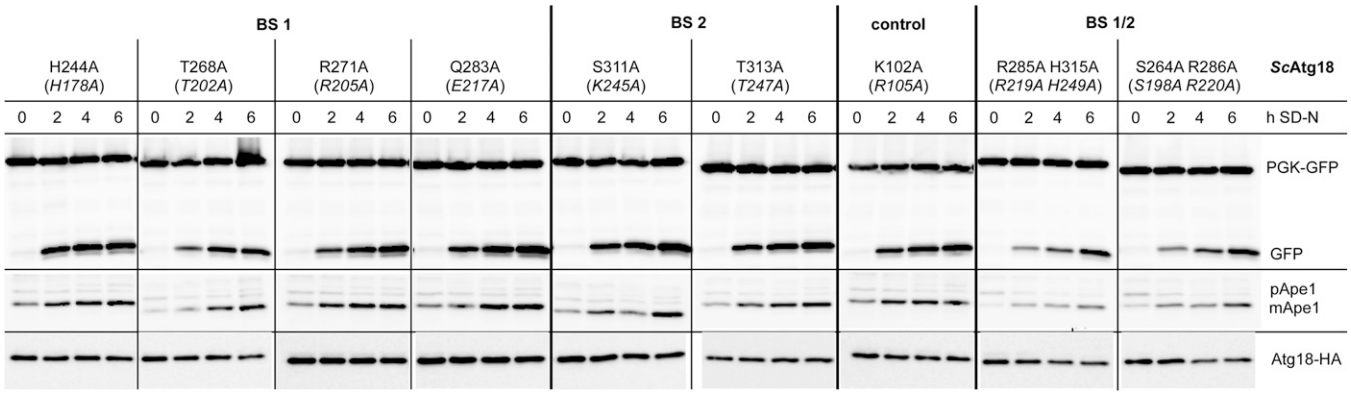

Fig. S6. Analysis of the functional relevance of conserved residues for macroautophagy. Cells deleted for *ATG18* and cotransformed with pRS316-PGK1-GFP and the indicated Atg18-HA mutants are grown to stationary phase in selection medium and shifted for 6 h to SD-(N) medium to induce macroautophagy. Samples were taken every 2 h. Quantifications are shown in Fig. 4. (*Top*) PGK1-GFP and free GFP are detected using a GFP-antibody to determine the amount of free GFP representing the autophagic rate. (*Middle*) Samples are reprobed to follow the cytoplasm-to-vacuole targeting (Cvt) pathway using a polyclonal Ape1 antibody to detect pApe1 and mApe1. (*Bottom*) Samples are reprobed using an HA antibody to demonstrate stability of the Atg18-HA proteins.

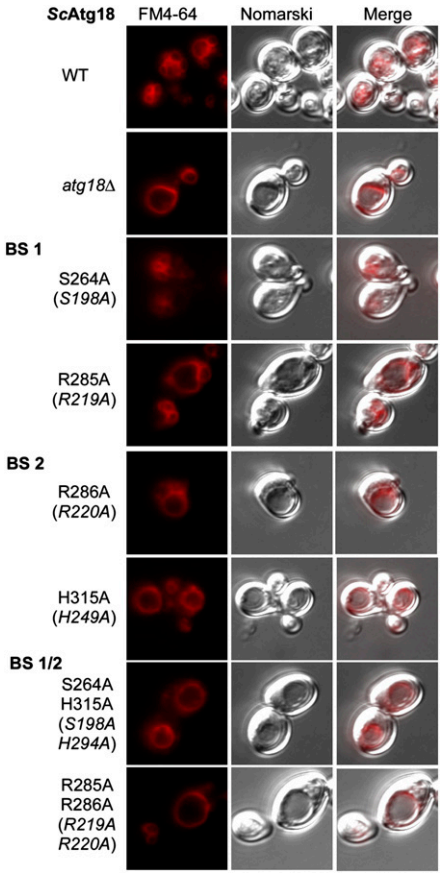

Fig. S7. Influence of the two binding sites on vacuole homeostasis, a PtdIns(3,5)P_2-dependent nonautophagic function of ScAtg18. Vacuoles are normally small and multilobed. A single unlobed and enlarged vacuole is a characteristic phenotype of *atg18*Δ cells. The *atg18*Δ*::kanMX6* cells of the *S. cerevisiae* BY4741 background were transformed with the indicated pRS313-Atg18-HA constructs. The vacuolar membrane was stained using FM4-64. Pictures were taken using a Zeiss Axioskope 2 with the FITC filter set and an AxioCam MRm camera and AxioVision software (version 4.5; Zeiss). The Atg18-HA WT protein complemented the enlarged vacuole phenotype. The single mutants in binding site 1 (Atg18^{S264A}-HA and Atg18^{R285A}-HA) and single mutants in binding site 2 (Atg18^{H315A} HA and Atg18^{R286A}-HA) only partially rescued the altered vacuole morphology. Double mutants (S264A H315A and R264A R265A) failed to complement.

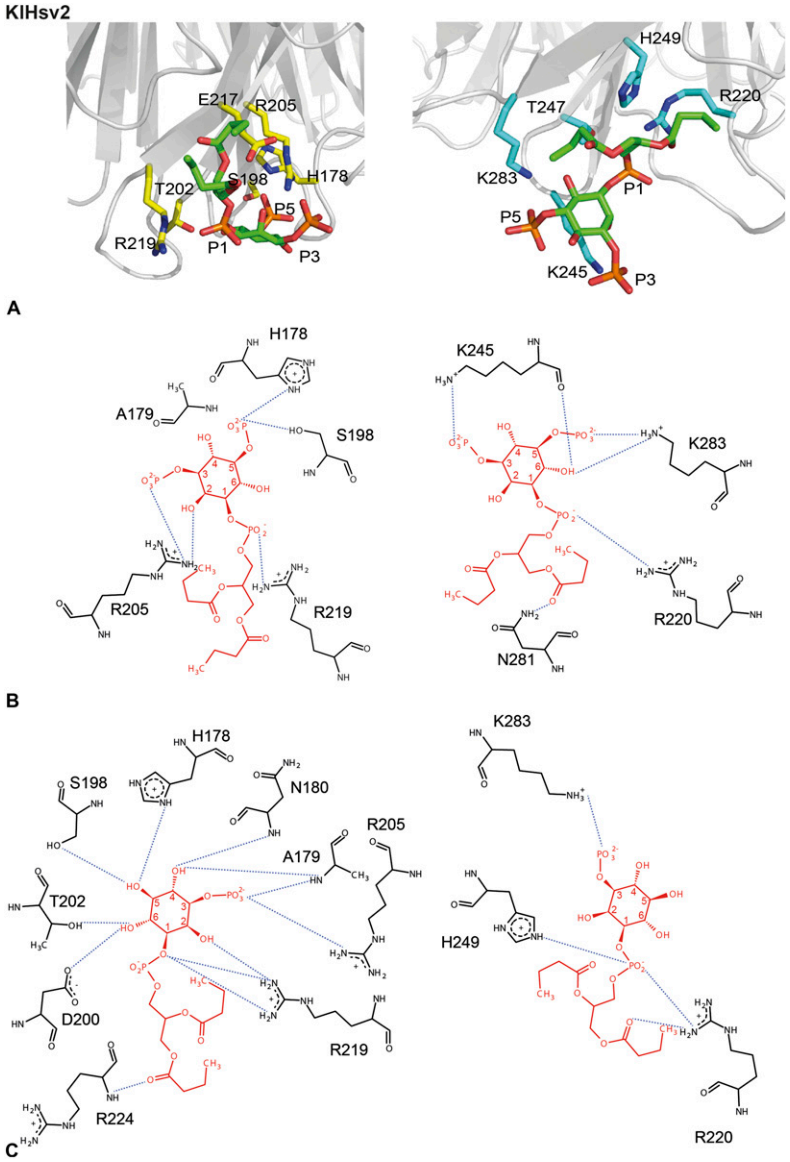

Fig. S8. Docking of PtdIns(3,5)P_2 into KlHsv2. (*A*) PtdIns(3,5)P_2 docked into binding sites 1 (*Left*) and 2 (*Right*) of KlHsv2. Residues important for phosphatidylinositol phosphate (PIP) binding are shown in yellow for binding site 1 and cyan for site 2. (*B*) Schematic diagrams show the details of protein and PtdIns(3,5)P_2 interactions. (*C*) Schematic diagrams show the details of protein and PtdIns3P interactions. Site 1 (*Left*) and the site 2 (*Right*) are shown. Salt bridges and hydrogen bonds are depicted with blue dashed lines. Hydrophobic interactions are not shown.

Table S1. Supplementary primer list

OEP-Atg18 SalI for	ttacggcgggcGTCGACCACATAGCGAGCTATGAAAAGATG
OEP-Atg18 EcoRI rev	ctattagcGAATTCTTAGCCGGCGTAATCCGGCAC
GFP-Ygr223c for	aatattaGGATCCATGGATGTTCGTCGACCTATAAG
GFP-Ygr223c rev	aatattaCTCGAGTTAAAGCTCTCTCCATGATTCTC
GFP-Atg18 Eco for	cgggctgcagGAATTCATGTCTGATTCATCACCTACTATC
GFP-Atg18 Xho rev	cgggctgcagCTCGAGTCAATCCATCAAGATGGAATACTG
ATG18 K102A for	CTTCTATTCTGAGTGTGAAAATGAATgcGTCTCGATTGGTGGTAC
ATG18 K102A rev	GTACCACCAATCGAGACgcATTCATTTTCACACTCAGAATAGAAG
ATG18 H244A for	CAACCATGGTCATCGAAGCTgcTAAGGGCGAGATTGCTGCAATGG
ATG18 H244A rev	CCATTGCAGCAATCTCGCCCTTAgcAGCTTCGATGACCATGGTTG
ATG18 S264A for	GACACTAATGGCTACCGCCgCTGATAAAGGTACTATCATCAG
ATG18 S264A rev	CTGATGATAGTACCTTTATCAGcGGCGGTAGCCATTAGTGTC
ATG18 T268A for	CCGCCTCTGATAAAGGTgCTATCATCAGGGTCTTTGAC
ATG18 T268A rev	GTCAAAGACCCTGATGATAGcACCTTTATCAGAGGCGG
ATG18 R271A for	CCTCTGATAAAGGTACTATCATCgcGGTCTTTGACATTGAAACGG
ATG18 R271 rev	CCGTTTCAATGTCAAAGACCgcGATGATAGTACCTTTATCAGAGG
ATG18 Q283A 2 for	GACATTGAAACGGGTGATAAGATCTACgcATTCAGGAGAGGGAC
ATG18 Q283A rev	CGTACGTCCCTCTCCTGAATgcGTAGATCTTATCACCCGTTTC
ATG18 R285A for	GGTGATAAGATCTACCAATTCgcGAGAGGGACGTACGCGAC
ATG18 R285A rev	GTCGCGTACGTCCCTCTCgcGAATTGGTAGATCTTATCACC
ATG18 R286A 2 for	GGGTGATAAGATCTACCAATTCAGGgcAGGGACGTACGCGAC
ATG18 R286A rev	CTTGTCGCGTACGTCCCTgcCCTGAATTGGTAGATCTTATCAC
ATG18 S311A for	CTTGGCGGTTACCGGCTCTgCCAAAACCGTGCATATCTTC
ATG18 S311A rev	GAAGATATGCACGGTTTTGGcAGAGCCGGTAACCGCCAAG
ATG18 T313A for	GGTTACCGGCTCTTCCAAAgCCGTGCATATCTTCAAATTGG
ATG18 T313A rev	CCAATTTGAAGATATGCACGGcTTTGGAAGAGCCGGTAACC
ATG18 H315A for	CCGGCTCTTCCAAAACCGTGgcTATCTTCAAATTGGGGCATTC
ATG18 H315A rev	GAATGCCCCAATTTGAAGATAgcCACGGTTTTGGAAGAGCCGG
ATG18 R285A R286A for	GGTGATAAGATCTACCAATTCgcGgcAGGGACGTACGCGAC
ATG18 R285A R286A rev	GTCGCGTACGTCCCTgcCgcGAATTGGTAGATCTTATCACC
ScHsv2 R123A for	CCATTAAAGACGTGTTTTTATCTgcGATTCATATTGTGGTAGTCCTGG
ScHsv2 R123A rev	CCAGGACTACCACAATATGAATCgcAGATAAAAACACGTCTTTAATGG
ScHsv2 H223H for	GCCCACTTCCATCATTAAAGCAgcTAAAAATCCCATCAAACTGGTT
ScHsv2 H223H rev	AACCAGTTTGATGGGATTTTTAgcTGCTTTAATGATGGAAGTGGGC
ScHsv2 S243A for	CACCATGGTAGCAACATGTgCCGTCCAGGG
ScHsv2 S243A rev	CCCTGGACGGcACATGTTGCTACCATGGTG
ScHsv2 T247A for	ACATGTTCCGTCCAGGGTgCACTTATAAGAATCTTCAG
ScHsv2 T247A rev	CTGAAGATTCTTATAAGTGcACCCTGGACGGAACATGT
ScHsv2 R250A for	GTTCCGTCCAGGGTACACTTATAgcAATCTTCAGTACGCATA
ScHsv2 R250A rev	TATGCGTACTGAAGATTgcTATAAGTGTACCCTGGACGGAAC
ScHsv2 E262A for	CATAACGGTACTTTAATCAAAGcATTTAGAAGAGGGGTGGACAAG
ScHsv2 E262A rev	CTTGTCCACCCCTCTTCTAAATgCTTTGATTAAAGTACCGTTATG
ScHsv2 R264A for	ACGCATAACGGTACTTTAATCAAAGAATTTgcAAGAGGGGTGGACAAG
ScHsv2 R264A rev	CTTGTCCACCCCTCTTgcAAATTCTTTGATTAAAGTACCGTTATGCGT
ScHsv2 R265A for	ATAACGGTACTTTAATCAAAGAATTTAGAgcAGGGGTGGACAAGGC
ScHsv2 R265A rev	GCCTTGTCCACCCCTgcTCTAAATTCTTTGATTAAAGTACCGTTAT
ScHsv2 K290A for	GGTAGTAAGTTGGCCGTATTGTCAAATgcGCAAACATTGCATATTTTCCAAA
ScHsv2 K290A rev	TTTGGAAAATATGCAATGTTTGCgcATTTGACAATACGGCCAACTTACTACC
ScHsv2 T292A for	TTGGCCGTATTGTCAAATAAGCAAgCATTGCATATTTTCCAAATTTTTGA
ScHsv2 T292A rev	TCAAAAATTTGGAAAATATGCAATGcTTGCTTATTTGACAATACGGCCAA
ScHsv2 H294A for	GCCGTATTGTCAAATAAGCAAACATTGgcTATTTTCCAAATTTTTGAAACAACCAA
ScHsv2 H294A rev	TTGGTTGTTTCAAAAATTTGGAAAATAgcCAATGTTTGCTTATTTGACAATACGGC
ScHsv2 FTTG for	GCATAACGGTACTTTAATCAAAGAATTTAcAAcAGGGGTGGACAAGGC
ScHsv2 FAAG for	AACGGTACTTTAATCAAAGAATTTGCAgcAGGGGTGGACAAGG
ScHsv2 FAAG rev	CCTTGTCCACCCCTgcTGCAAATTCTTTGATTAAAGTACCGTT

Primers are from Eurofins MWG Operon.